Supporting Information

Jung et al. 10.1073/pnas.1303916110

SI Materials and Methods

Wound-Healing Assay. Primary mouse embryonic fibroblast (MEF) cells were plated in 24-well plates with glass coverslips and grown to confluency. Cells were then scraped with a sterile p1000 pipette tip, washed with PBS, and incubated with fresh culture medium at 37 °C for 4 h. Cells were then fixed and stained for immunofluorescence microscopy.

Protein Sequence Alignment. Protein sequences of mouse lamin B1 (ENSMUSP00000025486) and mouse lamin B2 (ENSMUSP00000136524) were aligned using Clustal Omega (v1.1.0) with the default setting (www.ebi.ac.uk/Tools/msa/clustalo/).

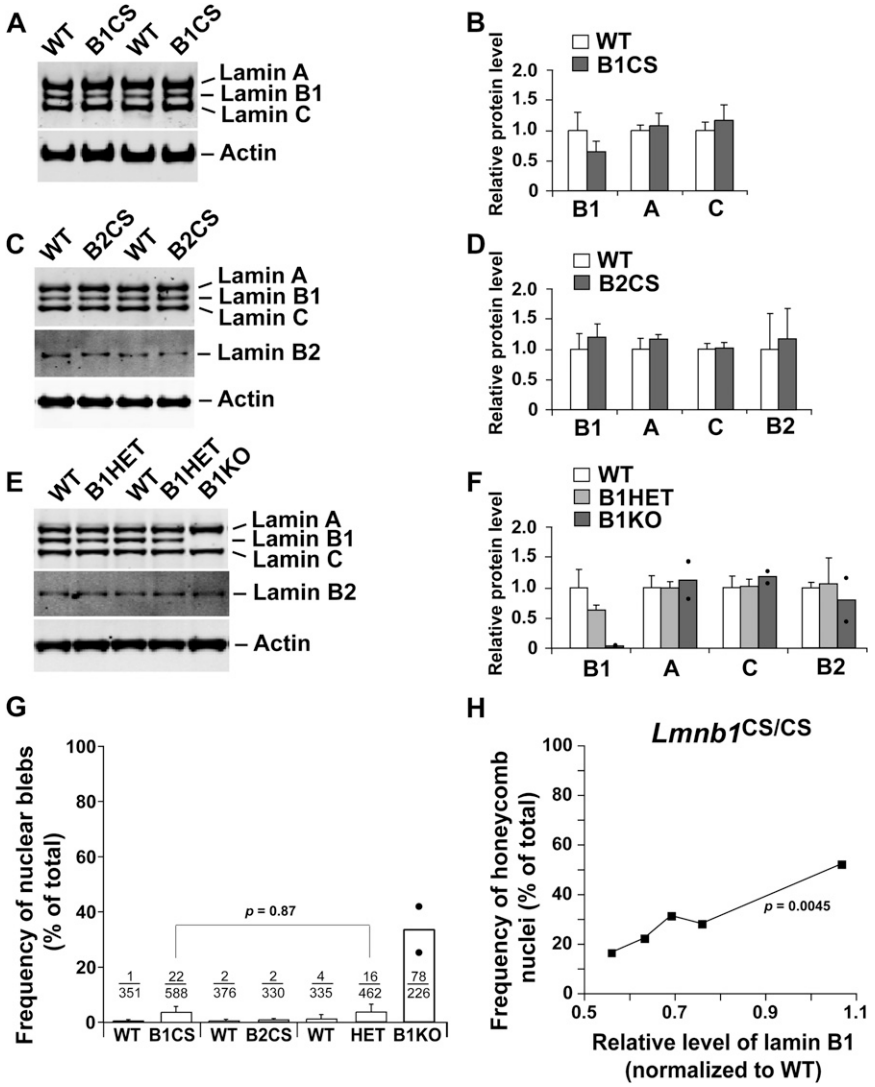

Fig. S1. Levels of nuclear lamin proteins and nuclear shape abnormalities in *Lmnb1*$^{CS/CS}$ and *Lmnb2*$^{CS/CS}$ MEFs. (*A*–*F*) Western blots (*A*, *C*, *E*) and quantification of lamin protein levels relative to actin (*B*, *D*, *F*) in WT, *Lmnb1*$^{CS/CS}$ (B1CS), *Lmnb2*$^{CS/CS}$ (B2CS), *Lmnb1*$^{+/-}$ (B1HET), and *Lmnb1*$^{-/-}$ (B1KO) MEFs (mean ± SD). The levels of lamin B1 in *Lmnb1*$^{CS/CS}$ MEFs were ∼35% lower than in wild-type cells (*B*) ($P = 0.06$) and similar to levels of lamin B1 in *Lmnb1*$^{+/-}$ cells (*F*) (where the levels were ∼37% lower than in wild-type cells; $P = 0.06$). (*G*) Frequency of nuclear blebs in the MEFs that were analyzed in Fig. 2 *A*–*F*. The frequency of nuclear blebs in *Lmnb1*$^{-/-}$ MEFs was higher than in wild-type MEFs ($P < 0.0001$). Frequencies of blebs in *Lmnb1*$^{CS/CS}$ and *Lmnb1*$^{+/-}$ cells were similar ($P = 0.87$); both were higher than in wild-type cells ($P < 0.0001$). Values represent mean ± SD. (*H*) Correlation between levels of nonfarnesylated lamin B1 and the frequency of honeycomb nuclei. Each point represents five individual *Lmnb1*$^{CS/CS}$ MEF cell lines (used in *G* and Fig. 2*G*). The frequency of honeycomb nuclei in *Lmnb1*$^{CS/CS}$ MEFs was positively correlated with lamin B1 levels ($P = 0.0045$).

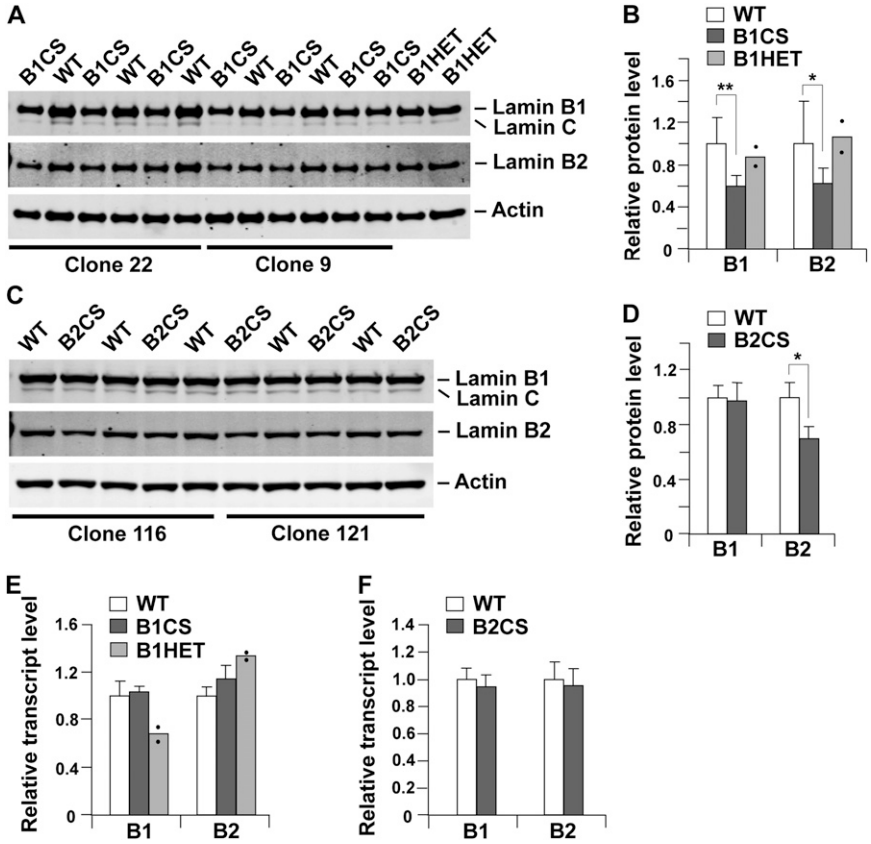

Fig. S2. Absence of the farnesyl lipid anchor lowers steady-state levels of lamin B1 and lamin B2 in the cortex. (*A* and *B*) Western blot analysis and quantification of lamin B1 and B2 levels in the cerebral cortex of embryonic day (E) 19 to postnatal day (P) 1 *Lmnb1*$^{+/+}$ (WT), *Lmnb1*$^{CS/CS}$ (B1CS), and *Lmnb1*$^{+/-}$ (B1HET) mice. Lamin B1 and lamin B2 levels were normalized to actin levels. Lamin B1 levels were ∼40% lower in *Lmnb1*$^{CS/CS}$ mice than in wild-type mice; this was the case in knock-in mice derived from two different ES cell lines (clones 22 and 9). *Lmnb1*$^{+/+}$, $n = 5$; *Lmnb1*$^{CS/CS}$, $n = 7$; *Lmnb1*$^{+/-}$, $n = 2$. Values represent mean ± SD. $*P < 0.05$; $**P < 0.005$. (*C* and *D*) Western blot analysis and quantification of lamin B1 and lamin B2 levels in the cerebral cortex of E19–P1 *Lmnb2*$^{+/+}$ (WT) and *Lmnb2*$^{CS/CS}$ (B2CS) mice. Values represent mean ± SD *Lmnb2*$^{+/+}$, $n = 5$; *Lmnb2*$^{CS/CS}$, $n = 5$. Lamin B1 and lamin B2 levels were normalized to actin. Lamin B2 levels were ∼30% lower in *Lmnb2*$^{CS/CS}$ mice than in wild-type mice; this was the case in mice generated from two ES cell lines (clones 116 and 121). $*P < 0.005$. (*E* and *F*) Quantitative RT-PCR analysis of *Lmnb1* and *Lmnb2* transcript levels in the cerebral cortex of E19–P1 *Lmnb1*$^{+/+}$ (WT), *Lmnb1*$^{CS/CS}$ (B1CS), *Lmnb1*$^{+/-}$ (B1HET), *Lmnb2*$^{+/+}$ (WT), and *Lmnb2*$^{CS/CS}$ (B2CS) mice. Transcript levels were normalized to cyclophilin A and compared with levels in wild-type mice (set at 1.0). Values represent mean ± SD. *Lmnb1*$^{+/+}$, $n = 5$; *Lmnb1*$^{CS/CS}$, $n = 7$; *Lmnb1*$^{+/-}$, $n = 2$; *Lmnb2*$^{+/+}$, $n = 5$; *Lmnb2*$^{CS/CS}$, $n = 5$.

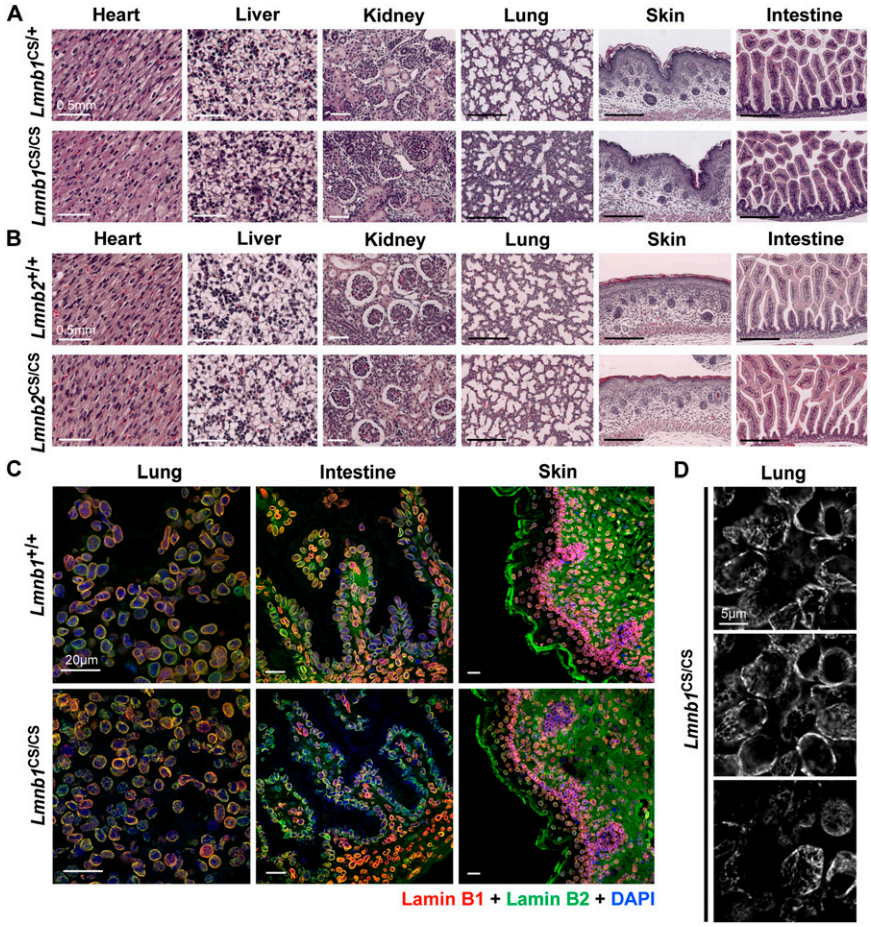

Fig. S3. Histological and immunohistochemical examination of tissues from *Lmnb1*$^{CS/CS}$ and *Lmnb2*$^{CS/CS}$ embryos. (*A* and *B*) H&E staining of the heart, liver, kidney, lung, skin, and intestine from *Lmnb1*$^{CS/+}$, *Lmnb1*$^{CS/CS}$, *Lmnb2*$^{+/+}$, and *Lmnb2*$^{CS/CS}$ mice at E19–P1. The lungs of *Lmnb1*$^{CS/CS}$ mice appeared immature with fewer alveoli and thicker interstitial spaces as described earlier in *Lmnb1* knockout mice (1). No pathology was detected in the other tissues. (Scale bars, 0.5 mm.) (*C*) Immunofluorescence microscopy of the lung, intestine, and skin from *Lmnb1*$^{+/+}$ and *Lmnb1*$^{CS/CS}$ embryos (E19–P1). Frozen tissue sections were stained with antibodies against lamin B1 (red) and lamin B2 (green). DNA was stained with DAPI (blue). Images along the *z* axis were captured and merged with Zen 2010 software (Zeiss). Both lamin B1 and lamin B2 were located mainly at the nuclear rim in the skin of *Lmnb1*$^{CS/CS}$ embryos. The cell nuclei in the lung and intestine of *Lmnb1*$^{CS/CS}$ mice exhibited a honeycomb distribution of B-type lamins (similar to the finding in MEFs) (Fig. 2*E*). (Scale bars, 20 μm.) (*D*) Higher-magnification images of individual optical sections of the lung from *Lmnb1*$^{CS/CS}$ mice illustrating the nuclear honeycomb phenotype. The distribution of lamin B1 (white) within cells is shown. (Scale bar, 5 μm.)

1. Vergnes L, Péterfy M, Bergo MO, Young SG, Reue K (2004) Lamin B1 is required for mouse development and nuclear integrity. *Proc Natl Acad Sci USA* 101(28):10428–10433.

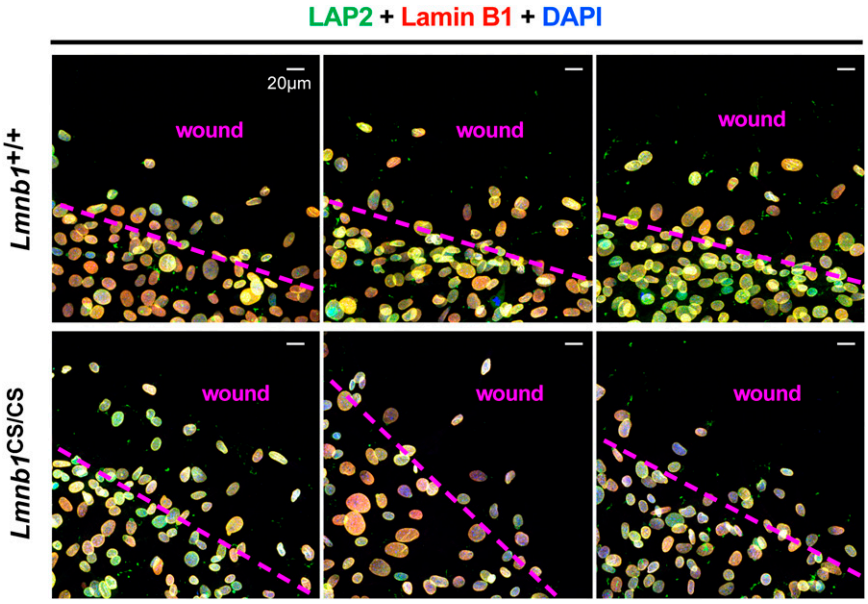

Fig. S4. Wound-healing assay with *Lmnb1*$^{+/+}$ and *Lmnb1*$^{CS/CS}$ MEFs. Confluent monolayers were scraped, with the goal of visualizing cells that migrate in and close the "wound." Cells were stained with antibodies against LAP2β (lamin-associated polypeptide 2; green) and lamin B1 (red); DNA was stained with DAPI (blue). The edge of the initial wound is indicated with a dashed line (magenta). The shapes of cell nuclei in migrating *Lmnb1*$^{CS/CS}$ MEFs were essentially normal, and no dumbbell-shaped nuclei were observed. (Scale bars, 20 μm.)

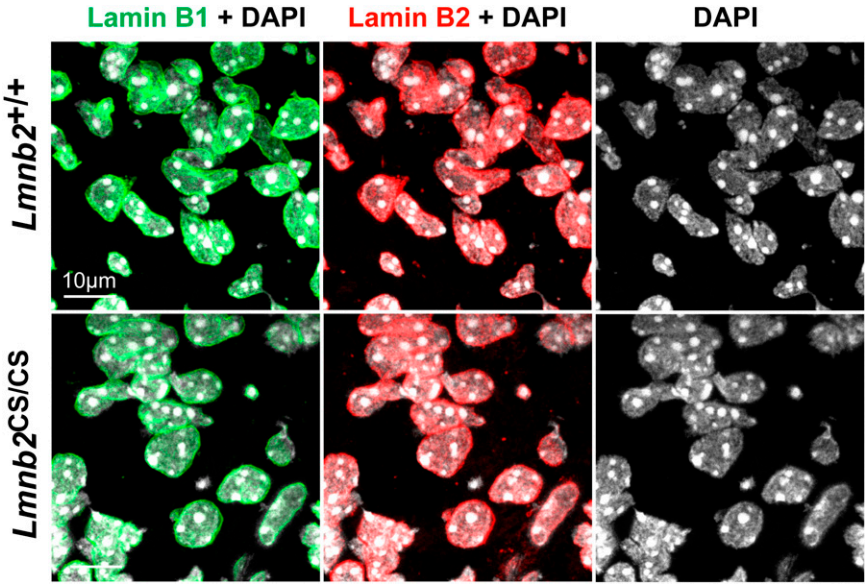

Fig. S5. Immunofluorescence microscopy of the midbrain (superior colliculus) from E19–P1 *Lmnb2*$^{+/+}$ and *Lmnb2*$^{CS/CS}$ embryos. Sections were stained with antibodies against lamin B1 (green) and lamin B2 (red); DNA was stained with DAPI (white). No dumbbell-shaped nuclei and naked chromatin were observed in *Lmnb2*$^{CS/CS}$ midbrains. (Scale bar, 10 μm.)

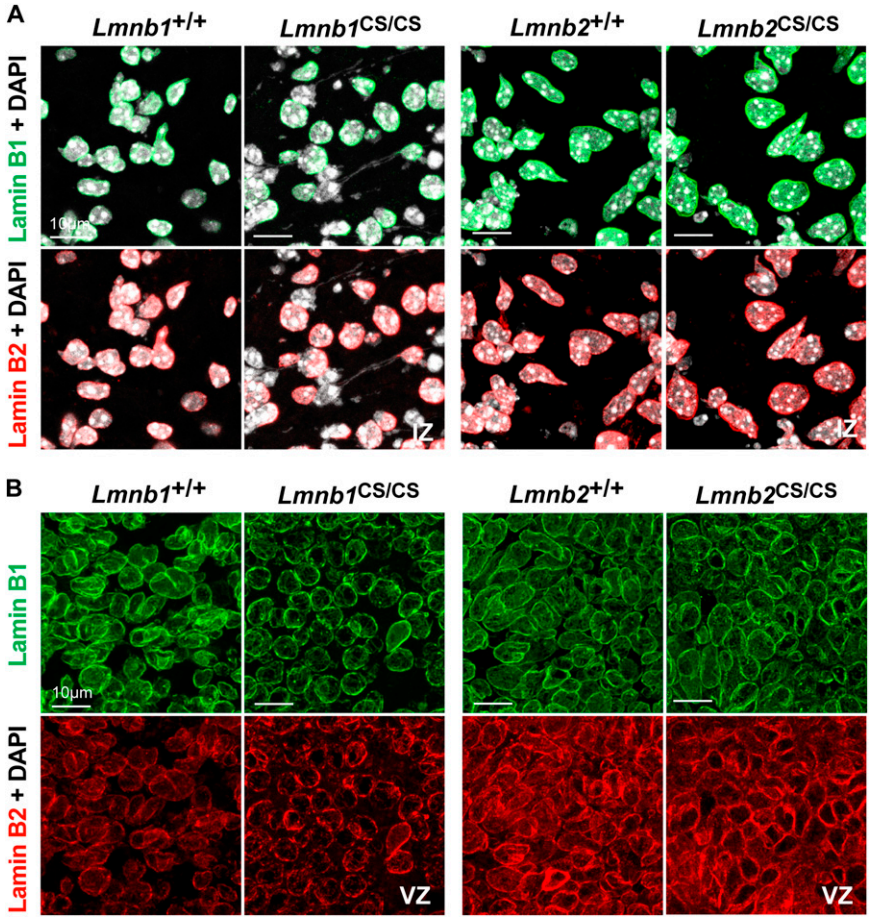

Fig. S6. Immunofluorescence microscopy of the cerebral cortex from E19–P1 *Lmnb1*$^{+/+}$, *Lmnb1*$^{CS/CS}$, *Lmnb2*$^{+/+}$, and *Lmnb2*$^{CS/CS}$ embryos. Frozen sections were stained with antibodies against lamin B1 (green) and lamin B2 (red); DNA was stained with DAPI (white). (*A*) Intermediate zone (IZ) of the cerebral cortex, showing dumbbell-shaped nuclei and "naked chromatin" in *Lmnb1*$^{CS/CS}$ embryos. (*B*) Ventricular zone (VZ), showing honeycomb distribution of lamin B1 in *Lmnb1*$^{CS/CS}$ embryos. No nuclear abnormalities were found in *Lmnb2*$^{CS/CS}$ embryos. (Scale bars, 10 μm.)

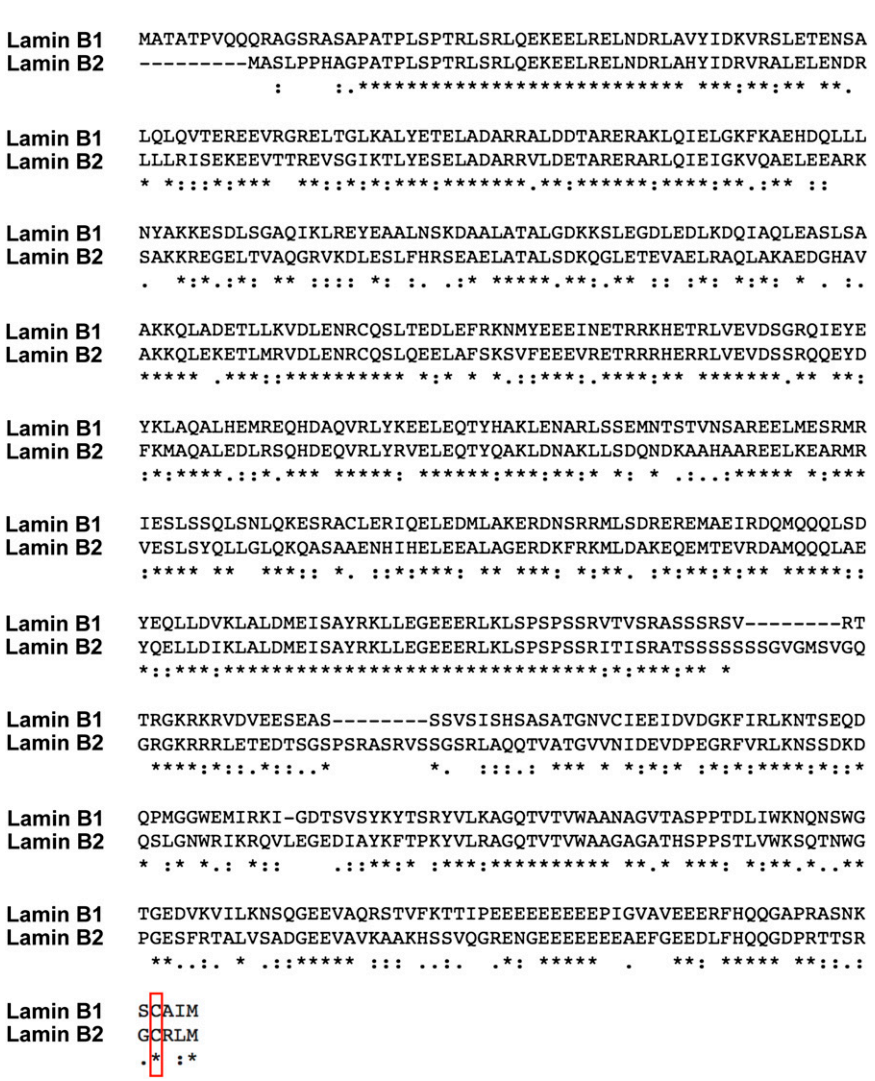

Fig. S7. Amino acid sequence alignment of mouse lamin B1 and lamin B2. An asterisk (*) represents a fully conserved residue; a colon (:) represents a residue with strongly similar properties; a period (.) represents a residue with weakly similar properties. The position of the "Cys-to-Ser" mutation in lamin B1 and lamin B2 are indicated with a red box.

Movie S1. EM tomography of the cerebral cortex of an *Lmnb1*$^{CS/CS}$ embryo illustrating a nuclear bleb surrounded by an inner and outer nuclear membrane. (See Fig. 8*D* for the scale bar.)

Movie S1